
FOUNDATIONS
ADVANCES

**Volume 72 (2016)**

**Supporting information for article:**

# A total scattering Debye function analysis study of faulted Pt nanocrystals embedded in a porous matrix

**Federica Bertolotti, Daniele Moscheni, Andrea Migliori, Stefano Zacchini, Antonio Cervellino, Antonietta Guagliardi and Norberto Masciocchi**

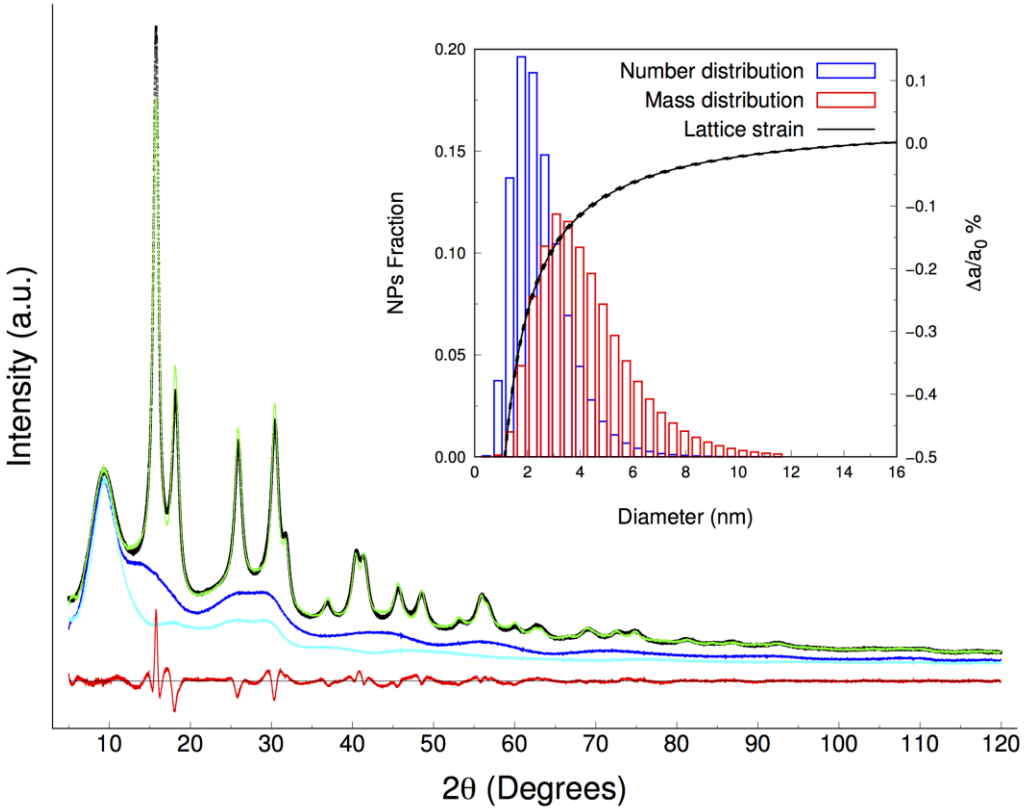


**Figure S1** Graphical output provided by the Debussy as results of the DFA analysis for the Pt@$SiO_2$-150C sample for a single SPH population model: best fit (green curve) of the WAXTS data (black points); blue and red curves describe the total background and the residual signals. The inset shows the number- and mass-based lognormal size distribution (left y-axis) and size-dependent lattice strain (right y-axis) (solid line; the ±1σ nearly overlapped dashed lines are derived from the uncertainty of the $\sigma_2$ parameter). This model provided mass-based average size parameters $\langle D \rangle_M$ = 4.201(3), $\sigma_M$ = 1.78(1), and lattice parameter $\langle a_k \rangle$ = 0.39167(1) nm. The large misfit of the 111 peak intensity suggested the occurrence of an additional phase morphologically elongated along this crystallographic direction.

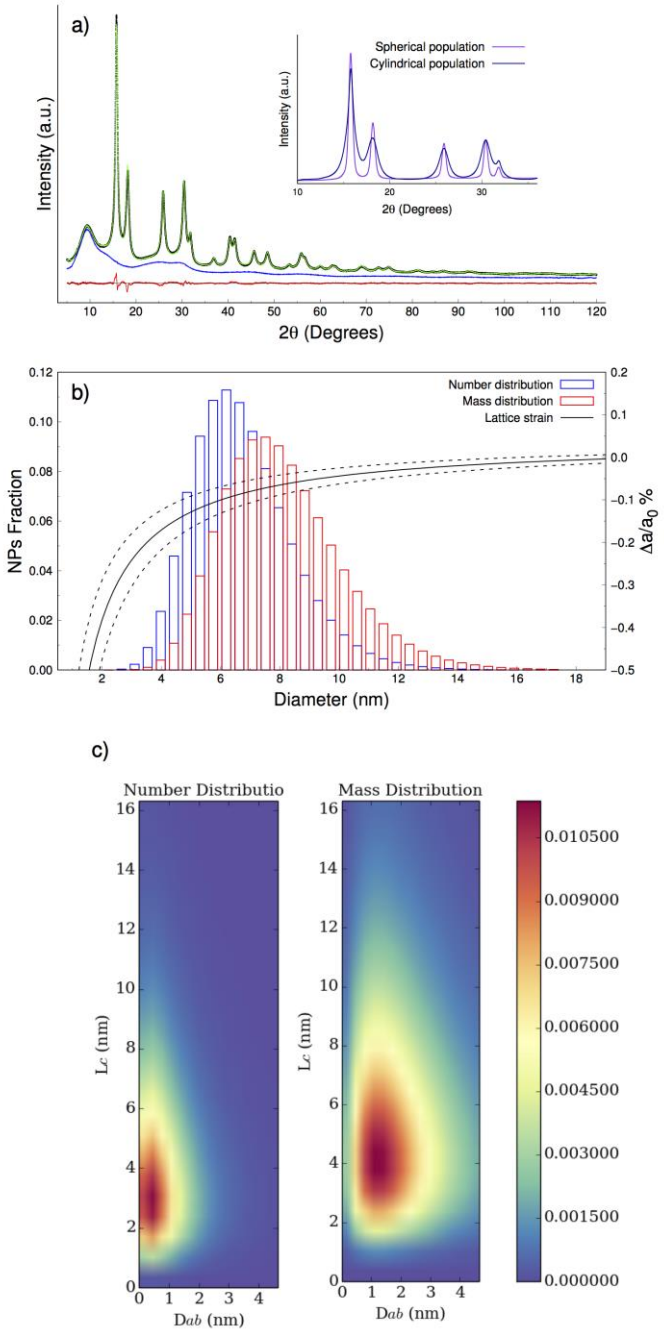


**Figure S2** Graphical output provided by the Debussy as results of the DFA analysis for the Pt@$SiO_2$-200C sample. **a**) Best fit (green curve) of the WAXTS data (black points); blue and red curves describe the total background and the residual signals. The inset shows the contribution to the overall intensity by the SPH and CYL populations of Pt NCs. **b**) Number- and mass-based lognormal size distribution (left y-axis) and size-dependent lattice strain (right y-axis) of the SPH NCs population (solid line). The ±1σ dashed lines are derived from the uncertainty of the $\sigma_2$ parameter. **c**) 2D maps of the number- and mass-based bivariate lognormal size distribution of the CYL population of NCs.

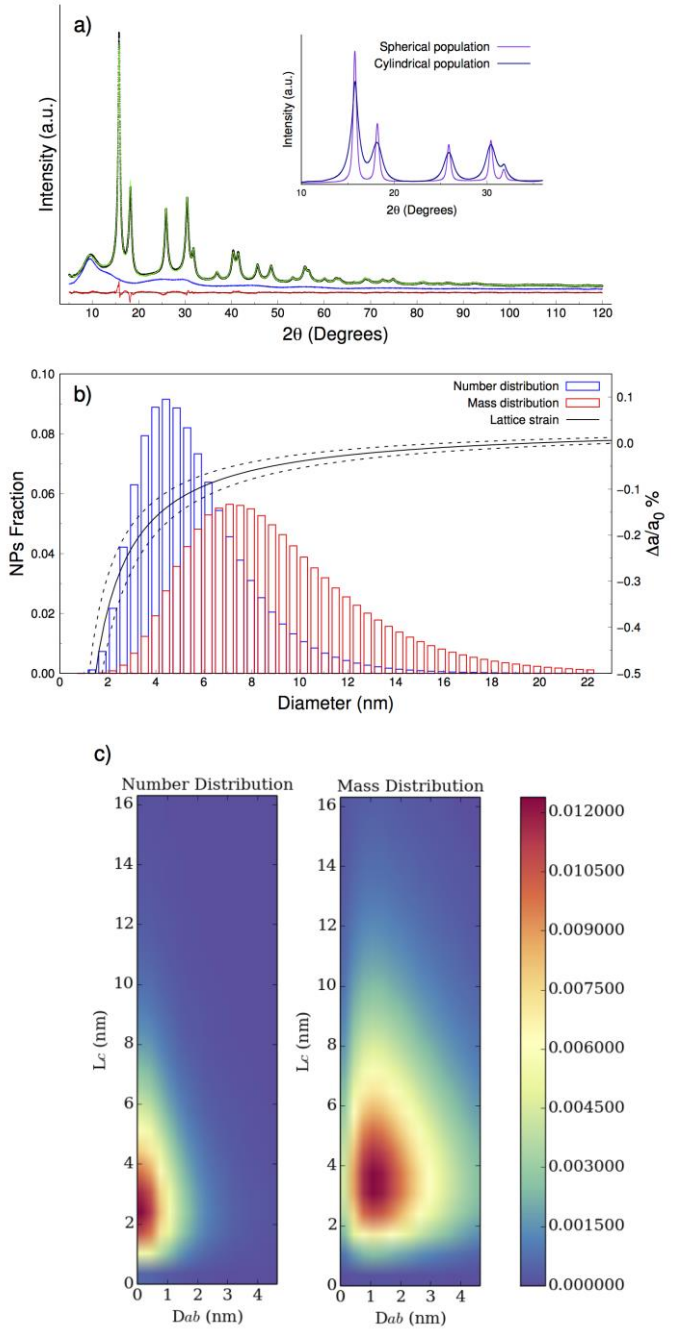


**Figure S3** Graphical output provided by the Debussy as results of the DFA analysis for the Pt@$SiO_2$-250C sample. **a**) Best fit (green curve) of the WAXTS data (black points); blue and red curves describe the total background and the residual signals. The inset shows the contribution to the overall intensity by the SPH and CYL populations of Pt NCs. **b**) Number- and mass-based lognormal size distribution (left y-axis) and size-dependent lattice strain (right y-axis) of the SPH NCs population (solid line). The $\pm1\sigma$ dashed lines are derived from the uncertainty of the $\sigma_2$ parameter. **c**) 2D maps of the number- and mass-based bivariate lognormal size distribution of the CYL population of NCs.

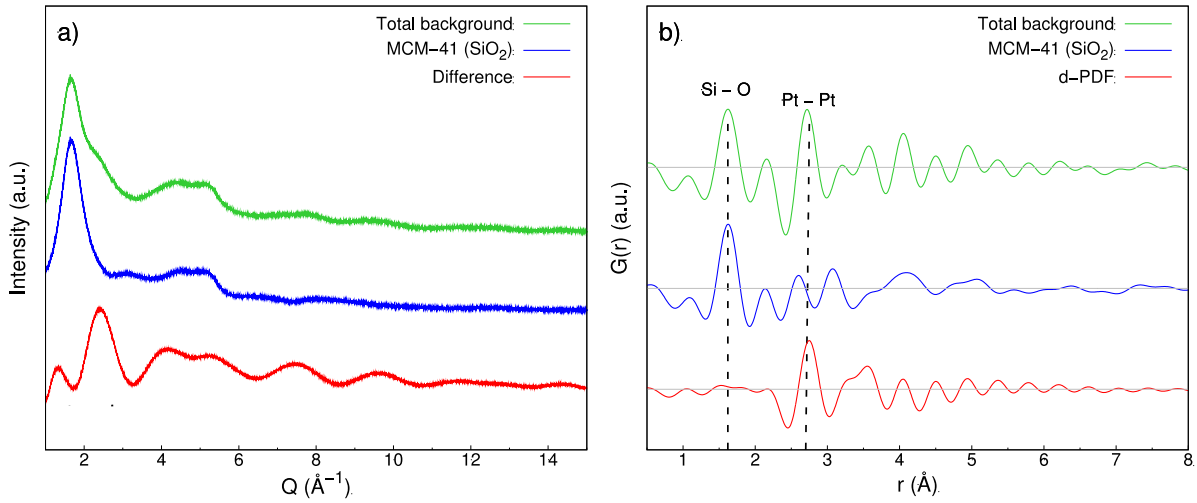


**Figure S4** - Pt@$SiO_2$-200C sample: **a**) Total background (green trace) and its two components in reciprocal space ($SiO_2$ MCM-41 in blue and the difference between the total and the *blank* signals, red trace); **b**) G(r) of the signals shown in **a**) highlighting the presence of a sub-nanometre Pt phase in the differential trace, as detailed in section 3.1 of the main text.

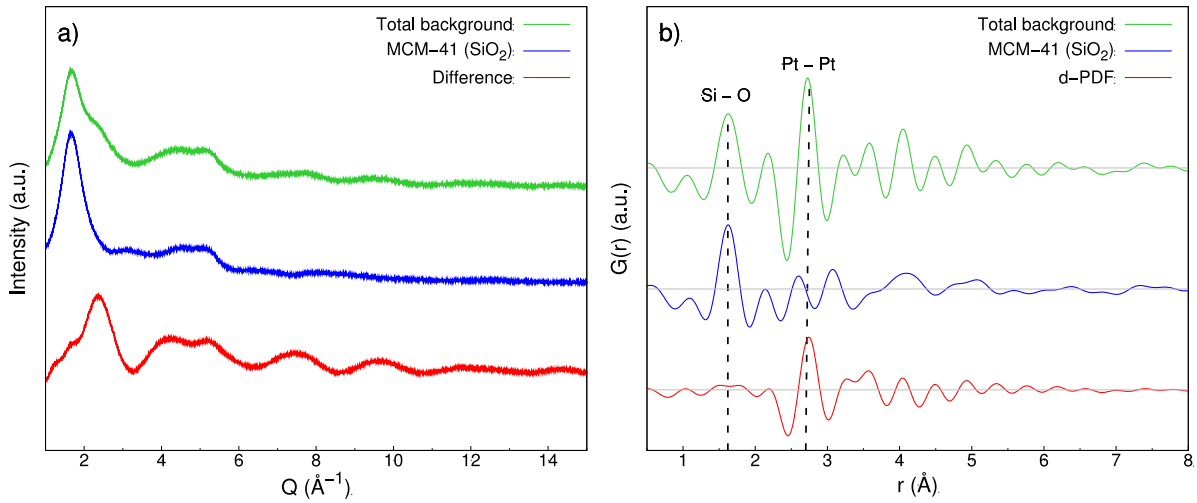


**Figure S5** Pt@$SiO_2$-250C sample: **a**) Total background (green trace) and its two components in reciprocal space ($SiO_2$ MCM-41 in blue and the difference between the total and the *blank* signals, red trace); **b**) G(r) of the signals shown in **a**).

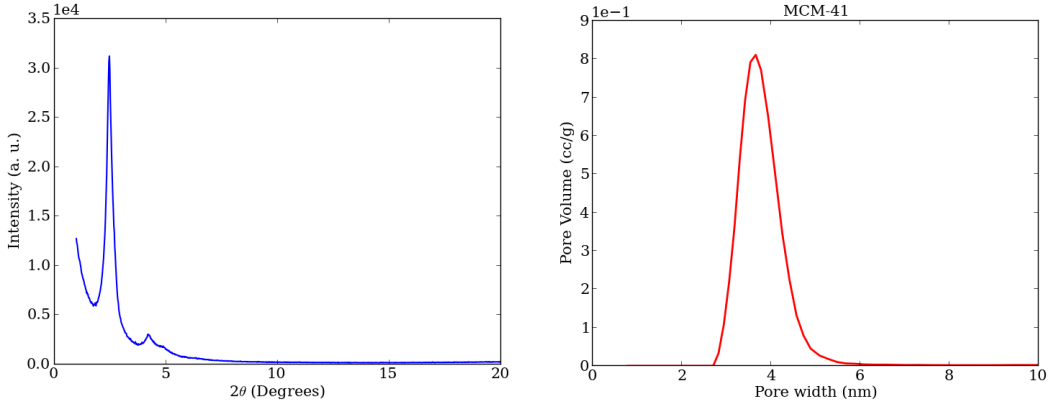


**Figure S6** Left: X-ray powder diffraction pattern collected on the nanoporous MCM-41 silica using a Bruker D8 Advance diffractometer (λ = 1.5418 Å). Peaks indicate the 2D organization of the channels. Right: B.E.T. curve showing the distribution of pore size in the silica matrix.

**Table S1** Relevant *number*-based averaged structural and microstructural features of the three Pt@$SiO_2$-150C, Pt@$SiO_2$-200C and Pt@$SiO_2$-250C samples derived from the DFA.

| **Sample** | **Pt@$SiO_2$-150C** | **Pt@$SiO_2$-200C** | **Pt@$SiO_2$-250C** |
|---|---|---|---|
| $\langle a_k \rangle$ (nm) (SPH) | 0.3917(1) | 0.3918(1) | 0.3917(1) |
| $\langle D \rangle_N$, $\sigma_N$ (nm) (SPH) | 4.79(1), 1.22(8) | 6.73(1), 1.68(9) | 5.61(1), 2.36(5) |
| $\langle D_{ab} \rangle_N$, $\sigma_{ab,N}$ (nm) (CYL) | 1.35(8), 0.5(2) | 1.3(1), 0.7(2) | 1.3(1), 0.7(1) |
| $\langle L_c \rangle_N$, $\sigma_{c,M}$ (nm) (CYL) | 3.42(1), 2.41(3) | 5.00(1), 2.74(5) | 4.34(1), 2.47(4) |
| Aspect Ratio, $\langle L_c \rangle_N / \langle D_{ab} \rangle_N$ | 2.5 | 3.7 | 3.4 |

**Table S2** *Mass*–based structural and microstructural parameters of the unfaulted model for Pt@$SiO_2$-150C, Pt@$SiO_2$-200C and Pt@$SiO_2$-250C samples.

| **Sample** | **Pt@$SiO_2$-150C** | **Pt@$SiO_2$-200C** | **Pt@$SiO_2$-250C** |
|---|---|---|---|
| GoF | 3.41 | 3.05 | 3.06 |
| $\langle a_k \rangle$ (nm) (SPH) | 0.3916(3) | 0.3921(4) | 0.3921(1) |
| $a_k$ (nm) (CYL) | 0.3919(-) | 0.3920(-) | 0.3919(-) |
| $\langle D \rangle_M$ , $\sigma_M$ (nm) (SPH) | 5.29(2), 1.5(1) | 7.82(2), 2.5(1) | 9.33(2), 3.22(9) |
| $\langle D_{ab} \rangle_M$ , $\sigma_{ab,M}$ (nm) (CYL) | 1.5(1), 0.6(4) | 2.1(3), 1.1(4) | 2.2(3), 1.1(3) |
| $\langle L_c \rangle_M$ , $\sigma_{c,M}$ (nm) (CYL) | 5.70(2), 3.08(5) | 6.99(1), 2.41(8) | 6.70(1), 2.94(6) |
| Aspect Ratio, $\langle L_c \rangle_M / \langle D_{ab} \rangle_M$ | 3.7 | 3.3 | 3.1 |
| Weight % (SPH) | 39.1 | 32.0 | 27.4 |